What can we learn from simulation-based quantification of energy dissipation in rockfall protection structures? Case of an articulated wall modelled with the NSCD method

Stéphane Lambert, Ritesh Gupta, Franck Bourrier, Vincent Acary

What can we learn from simulation-based quantification of energy dissipation in rockfall protection structures? Case of an articulated wall modelled with the NSCD method

Stéphane Lambert[1*], Ritesh Gupta[1], Franck Bourrier[1,2], Vincent Acary[2]

[1*]Univ. Grenoble Alpes, INRAE, CNRS, IRD, Grenoble INP, IGE Grenoble, 38000, France.
[2]Univ. Grenoble Alpes, Inria, CNRS, Grenoble INP, Institute of Engineering, LJK Grenoble, 38000, France.

Abstract

This article focus on the key issue of energy dissipation in passive rockfall protection structures when exposed to impact when intercepting a rock block. As an application case, a structure consisting in a wall made of articulated concrete blocks is considered. A Non-Smooth Contact Dynamics (NSCD) model of this structure was developed and calibrated with respect to the spatio-temporal impact response obtained from real-scale impact experiments. This model accounts for energy dissipation by friction between the system bodies and plasticization at contacts. The energy dissipation computation method is detailed and its correctness is demonstrated based on the simulation of two impact cases. The evolution with time of energy dissipation by each dissipative mechanism provides insights into the global structure response with time in terms of displacement and contact force amplitude. The influence of the model parameters on the contribution of these two dissipative mechanisms is evaluated. A ratio between energy dissipation by friction to energy dissipation by plasticization is proposed as a criterion for structural response evaluation. The variability in energy dissipation varying the impact conditions is addressed. In the end, this study reveals

the benefits derived from a precise quantification of energy dissipation in passive rockfall protection structures with promising perspectives in terms of structure design improvement.

Keywords: rockfall, impact, NSCD model, energy dissipation

1 Introduction

Passive rockfall protection structures such as flexible barriers, galleries, walls and embankments are often built on slopes to intercept or deviate rock blocks with kinetic energies sometimes exceeding 10 MJ (Volkwein et al, 2011). These protection structures are thus designed to withstand the severe localised dynamic loading they are exposed to during their normal operation. During impact, the structure experiences displacement and damage, with an amplitude that depends on the reduction in rock block kinetic energy over the impact duration. The kinetic energy lost by the rock block is progressively dissipated in the structure and, to a lesser extent, transferred to its foundation, this latter most often consisting in soil or bedrock.

The structure capacity in withstanding the impact load, as well as its mechanical response, is highly dependant on its capacity in transferring and dissipating energy. For this reason, energy dissipation in structures exposed to impacts by rock blocks is more and more addressed investigating the response of flexible barriers (Duan et al, 2023; Dhankal et al, 2012; Xu et al, 2018; Yu et al, 2019; Castanon-Jano et al, 2019; Di Giacinto et al, 2020; Previtali et al, 2021), embankments and walls (Ronco et al, 2009; Furet et al, 2022; Marchelli and Deangeli, 2022), steel posts (Zhao et al, 2021; Ng et al, 2023), cushion materials and energy dissipators (Zhang et al, 2017; Previtali et al, 2021; Yan et al, 2022; Liang et al, 2022; Yang et al, 2024). Dissipation in rockfall protection structures mainly results from plasticization of the structure materials and components and from friction within materials or at the interface between the structure components. Other dissipative mechanisms, such as thermal dissipation,

are generally negligible or considered as such. The prevailing dissipative mechanism depends on the structure type, its constitutive materials and design as well as on the incident rock block kinetic energy. The vast majority of research works addressing energy dissipation are based on simulation results, making use of commercially available or in-house codes which are based on finite element, finite difference or discrete element methods (FEM, FDM and DEM resp.). All these models rely on simplifications and assumptions in particular concerning the realism of the structure description and the considered constitutive laws. In the best case, the model parameters were calibrated and/or validated against results from experiments on real-scale structures.

By comparison with experiments, numerical simulations give a much easier access to the various data necessary for computing energy terms, and in particular the dissipative terms. Nevertheless, in all but a few research (e.g. (Ng et al, 2023)), the soundness of the energy terms quantification is debatable for various reasons. In many cases, not all the energy terms were taken into account. For example, elastic strain energy is often not mentioned, neither than the variation in potential energy, even when large mass components experience significant displacement along the vertical axis. Sometimes, the absence of the term is due to the fact that some commercially available simulation tools do not provide the user with all necessary data (e.g. Furet et al (2022); Yang et al (2024)).

In addition, very limited details are provided concerning the way the various energy terms were computed while the energy balance of the numerical method used can play an important role. Indeed, explicit schemes can inject artificial energy into the system if the time discretisation is too coarse. This problem is often avoided for reasons of computational stability by adding viscous dissipation to the system that is not justified by the physics of the phenomenon. Conversely, purely implicit schemes, such as the Euler backward scheme, dissipate a lot of energy numerically, which stabilises the numerical simulation but provides results that are not conducive to the safety of

protective structures. In the end, compliance with the fundamental principle of energy conservation in the system is rarely supported by evidences while it is a prerequisite for giving confidence in the simulation results. In many cases, this compliance is debatable or it can't be checked a posteriori (Di Giacinto et al, 2020).

This article proposes a detailed and rigorous investigation of energy dissipation in a particular and complex type of rockfall protection wall made from piled-up and articulated concrete blocks. This rockfall protection wall is first described. Then, the NSCD model implemented in the Siconos software, which meets energy conservation requirements thanks to a particular time integration scheme, and the method for computing energy dissipation from simulation results are presented. The detailed analysis of energy balance for two impact cases reveals the interest in considering dissipative mechanisms for describing the whole structure response with time. The influence of the model parameters and of the impact conditions on the structure response is then addressed, focusing on the respective contribution of the dissipative mechanisms. The ratio between the amount of energy dissipated by friction to that dissipated by plastification is then proposed and used for describing the whole structure response. Combined with the energy transferred to the structure, this ratio is proposed for improving the structure design when considering a wide range of impact conditions.

2 Considered rockfall protection structure and its model

This research focuses on a specific type of rockfall protection structure made of concrete blocks interconnected one to each other to form articulated walls. This type of massive rockfall protection structure has the advantage of having a reduced foot-print, similarly as other structures (Lambert et al, 2019; Korini et al, 2021). The development of this structure type involved real-scale impact experiments together with numerical modelling.

2.1 Structure description

The structure consists of concrete blocks, 1850kg in mass each, that are piled up in staggered rows (Fig. 1). Superimposed concrete blocks are traversed along the vertical axis by connectors consisting in assemblies of metallic tubes and cables which aim is to ensure mechanical continuity of the wall. The concrete blocks shape favours relative rotation between adjoining blocks in the same horizontal row. The wall deformation capacity is further increased by the space left between tubes and concrete blocks, on one side, and between adjoining concrete blocks on a same horizontal row on the other. This innovative technology offers the possibility to build massive vertical walls, with reduced foot print, high deformability and versatility. For example, different geometric arrangement of the concrete blocks along the longitudinal axis can be adopted such as the zig-zag pattern considered in this study or a linear wall, with or without partition walls (Furet et al, 2022). Such structures are intended to serve as passive protection against gravity driven natural hazards, and in particular rockfall. A key feature of this structure type lies in the fact that the interconnections between the concrete blocks improve the structure stability preventing from excessive concrete blocks displacements in the impact vicinity.

Depending on the kinetic energy of the rockfall to intercept, the impact response of such articulated-concrete blocks walls may involve concrete crushing and fracture, basal sliding, wall tilting and relative displacement between superimposed concrete blocks with an amplitude that decreases with the distance to the impact location (see (Furet et al, 2020, 2022; Gupta et al, submitted)).

More details concerning the structure description are provided in (Furet et al, 2022).

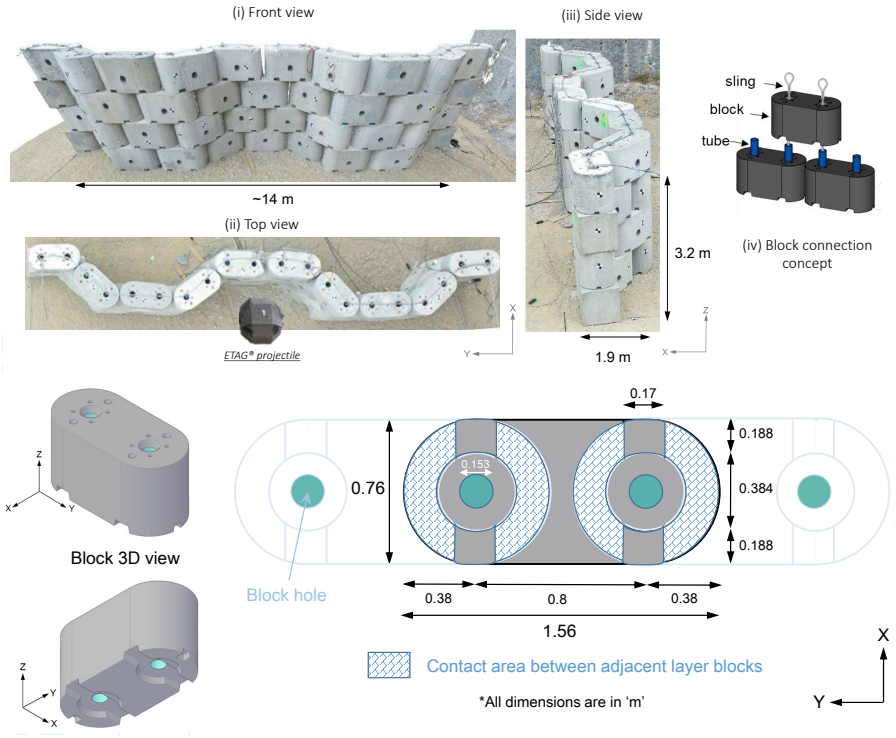

Fig. 1 (a) Experimental full-scale structure and (b) concrete block geometry and dimensions

2.2 The NSCD structure model

The structure was modelled using the Siconos software package (Acary and Perignon, 2007; Acary et al, 2019) which is based on the Non-Smooth Contact Dynamics (NSCD) approach (Jean and Moreau, 1987; Jean, 1999; Dubois et al, 2018). The choice of NSCD modelling was preferred over FEM, FDM and DEM for computation time reasons. With NSCD, one simulation with a personal computer typically lasted 20 minutes, compared to 10 hours with the finite difference model proposed by Furet et al (2022). Running thousands of simulations for example in view of investigating the structure response varying the parameters describing the structure or the impact conditions thus becomes affordable.

The layout of the wall model is presented in Figure 2 comprising of modelled components for blocks, connectors and projectile. The mechanical and geometrical properties of most of the components are directly taken from the full-scale experimental structure. However, five model parameters cannot be directly assigned. Three parameters concerned the contact mechanics, namely the restitution coefficient e, and two friction coefficients for concrete-concrete interfaces and concrete-foundation interface μ_{cc} and μ_{cs}. These three parameters are intrinsic to the modelling approach and are not easy to measure a reliable way under dynamic conditions. The two other parameters v_p and d_z concerned geometrical features used in the model for describing the structure. The parameter v_p represents the relative looseness in the cable connecting the concrete blocks and d_z defines the position of the virtual disk that enables the contact between the blocks and the tubes. The need for a calibration of these two parameters resulted from a large value variability and from a difficulty in determining a relevant and precise value from some measurements.

More details concerning the way the structure was represented are provided in Gupta et al (2023).

The main lines of the computation method are described in the following and an exhaustive description is given in Acary and Collins-Craft (2023), in the case of linear elasto-dynamics. In our context of 3D rigid bodies, the equation of motion with contact and Coulomb friction is given by:

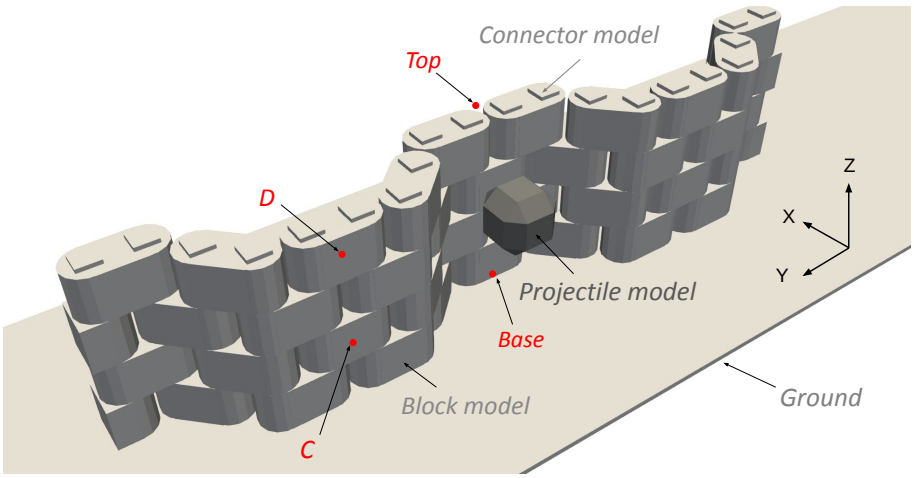

Fig. 2 The NSCD model of the articulated concrete block structure and its components, taken from (Gupta et al, 2023). Location of points where data were collected during the real-scale experiments ('Base', 'Top', 'C' and 'D').

$$
\left\{
\begin{array}{lll}
\dot{q} = T(q)v, & & \\
M\dot{v} = F(t,q,v) + G^{\top}(q)r, & & \\
u^{\alpha} = G^{\alpha}(q)v & & \\
r^{\alpha} = 0, & \text{if } g_{\mathrm{N}}^{\alpha}(q) > 0, & \\
K^{\alpha,*} \ni \widehat{u}^{\alpha} \perp r^{\alpha} \in K^{\alpha}, & \text{if } g_{\mathrm{N}}^{\alpha}(q) = 0, & \\
u_{\mathrm{N}}^{\alpha,+} = -e^{\alpha} u_{\mathrm{N}}^{\alpha,-}, & \text{if } g_{\mathrm{N}}^{\alpha}(q) = 0 \text{ and } u_{\mathrm{N}}^{\alpha,-} \leq 0 &
\end{array}
\right\} \alpha \in \mathcal{I},
$$

The vector q is the configuration vector which combines the position of the centre of mass and the parameterisation of the rotation with quaternions for each body. The generalised velocity vector v contains the centre of mass velocities and the angular velocities expressed in the body frame. The matrix $T(q)$ relates the time derivative of q to v. $\mathcal{I}$ is the set of potential contacts and $g_{\mathrm{N}}^{\alpha}(q)$ is the gap function associated to the distance between bodies potentially in contact. The matrix M is the mass matrix, the vector F is the force vector that collects the external applied forces and the gyroscopic

effects. For the contact point $\alpha \in \mathcal{I}$, the matrix $G^\alpha(q)$ is the contact configuration matrix, which expresses the local relative contact velocity u in terms of the generalised velocities v. The matrix $G(q)$ collects the matrices $G^\alpha(q)$ for $\alpha \in \mathcal{I}$.

The reaction forces r^α and the velocities u^α are decomposed into their normal and tangent parts, denoted $r_{\mathrm{N}}, r_{\mathrm{T}}$ and u_{N}, u_{T}, respectively.

Using the modified relative contact velocity $\widehat{u}^\alpha$, such that $\widehat{u}^\alpha_{\mathrm{N}} = u^\alpha_{\mathrm{N}} + \mu^\alpha \|u^\alpha_{\mathrm{T}}\|$, $\widehat{u}^\alpha_{\mathrm{T}}$ $= u^\alpha_{\mathrm{T}}$, the Coulomb friction with unilateral contact is expressed as (see Acary et al (2018) for details) :

$$K^{\alpha,*} \ni \widehat{u}^\alpha \perp r^\alpha \in K^\alpha, \tag{1}$$

The $x \perp y$ symbol means that $y^\top x = 0$. The cone $K = \{r \in I\!R^3, ||r_{\mathrm{T}}|| \leq \mu r_{\mathrm{N}}\}$ is the usual Coulomb friction cone and $K^* = \{z \in I\!R^3 \mid z^T x \geq 0 \text{ for all } x \in K\}$ its dual.

The formulation is completely equivalent to the standard Coulomb friction model with contact as shown in (Acary and Collins-Craft, 2023). The relation $u^{\alpha,+}_{\mathrm{N}} = -e^\alpha u^{\alpha,-}_{\mathrm{N}}$ is the Newton impact law for the contact α.

In order to take into account the impact phenomenon in case of a jump in velocity, in a way that is consistent with the energy dissipation, the contact law is written with the help of the Frémond approach Frémond (2017); Frémond (2002) as

$$K^{\alpha,*} \ni \begin{bmatrix} \bar{u}_{\mathrm{N}} + \frac{1}{2} e u^-_{\mathrm{N}} + \mu^\alpha \|\bar{u}^\alpha_{\mathrm{T}}\| \\ \bar{u}_{\mathrm{T}} \end{bmatrix} \perp p^\alpha \in K^\alpha, \tag{2}$$

where $\bar{u} = \frac{1}{2}(u^{\alpha,+} + u^{\alpha,-})$ is the average velocity of the pre- and post-impact velocities, and p^α the contact impulse.

With the Frémond approach, the Moreau–Jean scheme (with $\theta = 1/2$) for the system, for a time discretization $t_0 < \ldots < t_k < t_{k+1} < \ldots < t_n$ with a time step

$h = t_{k+1} - t_k$, is adapted as follows

$$\left\{\begin{array}{ll}
q_{k+1} = q_k + hT(q_{k+1/2})v_{k+1/2} & \\
M(v_{k+1} - v_k) - hF_{k+1/2} = G^\top(q_k)p_{k+1}, & \\
u_{k+1/2} = G(q_k)v_{k+1/2}, & \\
p^\alpha_{k+1} = 0, & \left.\right\} \alpha \notin \mathcal{I}_k \\
K^{\alpha,*} \ni \widetilde{u}^\alpha_{k+1/2} \perp p^\alpha_{k+1} \in K^\alpha & \left.\right\} \alpha \in \mathcal{I}_k.
\end{array}\right. \tag{3}$$

with

$$\widetilde{u}_{k+1/2} = \begin{bmatrix} u_{\mathrm{N},k+1/2} + \frac{1}{2}(e-1)u_{\mathrm{N},k} + \mu^\alpha \|u^\alpha_{\mathrm{T},k+1/2}\| \\ \bar{u}_{\mathrm{T},k+1/2} \end{bmatrix} \tag{4}$$

to be consistent with Equation (2). The standard notation $x_{k+1/2} = 1/2(x_k + x_{k+1})$ is used. The set $\mathcal{I}_k$ is the set of contacts activated at the velocity level:

$$\mathcal{I}_k = \{\alpha \in I \mid g^\alpha_{\mathrm{N},k} + \frac{1}{2}u^\alpha_{\mathrm{N},k} \leq 0, \text{ and } u^\alpha_{\mathrm{N},k} \leq 0\} \tag{5}$$

The Frémond approach differs from the more classical approach, which was in particular used by the authors in their previous work (Gupta et al, 2023, submitted), that consists in using the post-impact velocity $u^{\alpha,+}$ instead of $\bar{u}$. It was preferred in this study because preliminary simulations emphasized that the classical approach resulted in slight energy balance discrepancies in the rare case of a sliding velocity reversal during impact.

2.3 Model calibration

The calibration of the five model parameters was conducted based on a complex and innovative approach quantitatively minimising the model prediction error in terms of

wall impact response with time and space. This approached is described in Gupta et al (2023) and is briefed here.

The calibration made use of measures collected during two impact tests on real-scale structures, 14 m long and 3.2 m high. These impact tests involved a projectile 1.1 m in size with a kinetic energy at impact of 520 and 1020 kJ (Furet et al, 2022). The considered measurements were the displacement at four points in the structure, as illustrated in Figure 2, and at three times, i.e. for a total of 24 measures. Calibrating the model parameters against this set of data thus allows accounting for the whole structure response with time and space, under two different loading conditions.

The calibration strategy relied on the Bayesian interface statistical learning method, accompanied by the meta-modelling techniques. The meta-modelling techniques presented a surrogate of the NSCD model which represented a similar response albeit negligible computation time (microseconds) in comparison to the time for one NSCD model computation. Subsequently, a large number of computations was made possible by meta-models which served as a forward model of the Bayesian interface for model calibration. Besides, the Sobol sensitivity analysis was made possible through the surrogate model which presented the relative influence of one parameter to the other both in space and time.

This approach resulted in reference model parameter values presented in the first row of Table 1. These values slightly differ from that in Gupta et al (2023, submitted) due to the improvement in the computation scheme as detailed in section 2.2. Reference to the other rows of this table will be made in section 4.

The significant effort made for calibrating the five model parameters based on 24 data describing the spatio-temporal response of the structure is considered to give confidence in the model's predictive capacity. By contrast, it is thought that a calibration based on a smaller data set, as often done, would have resulted in a less efficient

model for predicting the whole structure response when varying the impact conditions for example.

Table 1 Parameters value of the different models used in this study

Model	d_z (cm)	v_p (cm)	μ_{cc} (-)	μ_{cs} (-)	e (-)
Reference	7.3	6.7	0.313	0.310	0.221
CS1	9.4	7.1	0.392	0.307	0.135
CS2	9.8	3.7	0.277	0.417	0.018
CS3	6.0	7.6	0.289	0.427	0.284
CS4	9.0	5.0	0.309	0.344	0.296
CS5	7.0	8.7	0.251	0.315	0.291
CS6	6.9	9.9	0.542	0.301	0.288
CS7	6.7	9.0	0.253	0.322	0.296
CS8	8.9	3.9	0.389	0.305	0.107
CS9	5.1	9.7	0.257	0.308	0.209

3 Energy dissipation computation

This section first introduces the method established for computing energy dissipation from the model simulation results. This method is then applied to two cases for its validation.

3.1 Energy terms computation

This section presents the way energy dissipation terms were computed.

The discrete kinetic energy is defined as

$$KE_{k+1} = \frac{1}{2} v_{k+1}^{\top} M v_{k+1}, \tag{6}$$

and the variation of energy due to the work of forces is defined as

$$\Delta_k^{k+1} PE = -h v_{k+1/2} F_{k+1/2}. \tag{7}$$

The notation $\Delta_k^{k+1} P$ is used to outline that the work of forces over a time interval is equal to the variation of the potential energy if the gyroscopic forces vanish.

The work associated with the normal component of a contact impulse is given by:

$$w_{\mathrm{N}}^{\alpha} = \frac{1}{2}(u_{\mathrm{N}}^{\alpha,+} + u_{\mathrm{N}}^{\alpha,-}) p_{\mathrm{N}}^{\alpha} = \frac{1}{2}(1 - e^{\alpha}) u_{\mathrm{N}}^{\alpha,-} p_{\mathrm{N}}^{\alpha} \leq 0 \tag{8}$$

since $u_{\mathrm{N}}^{\alpha,-} \leq 0$ and $p_{\mathrm{N}}^{\alpha} \geq 0$,

The work associated with the tangential component of a contact impulse is computed as:

$$w_{\mathrm{T}}^{\alpha} = \frac{1}{2}(u_{\mathrm{T}}^{\alpha,+} + u_{\mathrm{T}}^{\alpha,-}) p_{\mathrm{T}}^{\alpha} = -\mu^{\alpha} \|\bar{u}_{\mathrm{T}}\| p_{\mathrm{N}}^{\alpha} \leq 0. \tag{9}$$

The discrete work of all contact impulses is given by:

$$W_{k+1} = \sum_{\alpha \in I} u^{\alpha}_{k+1/2} p^{\alpha}_{k+1}, \tag{10}$$

that be decomposed in its normal

$$W_{\mathrm{N},k+1} = \sum_{\alpha \in I} u^{\alpha}_{\mathrm{N},k+1/2} p^{\alpha}_{\mathrm{N},k+1} = \sum_{\alpha \in I} \frac{1}{2}(1 - e^{\alpha}) u^{\alpha}_{\mathrm{N},k} p^{\alpha}_{\mathrm{N},k} \tag{11}$$

and tangent parts

$$W_{\mathrm{T},k+1} = \sum_{\alpha \in I} u^{\alpha}_{\mathrm{T},k+1/2} p^{\alpha}_{\mathrm{T},k+1} = \sum_{\alpha \in I} -\frac{1}{2}\mu^{\alpha} \| u^{\alpha}_{\mathrm{T},k+1} + u^{\alpha,-}_{\mathrm{T},k+1} \| p^{\alpha}_{\mathrm{N},k}. \tag{12}$$

It is shown in Acary and Collins-Craft (2023), in the case of linear elasto-dynamics, that the discrete work of contact forces is non positive and the following discrete energy balance is satisfied

$$\Delta KE^{k+1}_{k} + \Delta^{k+1}_{k} PE = W_{k+1}, \text{ with } W_{k+1} \leq 0. \tag{13}$$

where $\Delta K^{k+1}_{k} = K_{k+1} - K_k$. Numerical evidence shows this relation is also satisfied in the case of rigid bodies under gravity.

The energy dissipation due to the work of the tangential components of contact impulses ($W_{\mathrm{T},k+1}$) is directly related to frictional processes. Consequently, the cumulative energy dissipated by friction is :

$$D_f = -\sum_{k=0}^{N} W_{\mathrm{T},k+1} \geq 0. \tag{14}$$

The remaining part of the work of the contact impulses, that is the contribution of the normal components of contact impulses ($W_{\mathrm{N},k+1}$), is associated with energy

dissipation (D_p) due to plasticization in the concrete block, in particular in the vicinity of the impact point. D_p is defined as

$$D_p = -\sum_{k=0}^{N} W_{\mathrm{N},k+1} \geq 0, \tag{15}$$

Over the whole time interval of simulation, we have the energy balance

$$\Delta(KE + PE) = -(D_p + D_f). \tag{16}$$

In other words, the total energy of the system decreased over time by the amount of dissipation at contacts by friction and plasticization.

3.2 Application to the reference impact cases

The previously described method was used for computing energy dissipation in the case of the two impact tests conducted on the real-scale structures (Furet et al, 2022). The considered time step was 0.25 milliseconds and the duration was 1 second (see the video of a simulation with this link).

For both impact energies, Figure 3 shows the evolution with time of the kinetic energy and variation in potential energy of all the concrete blocks (KE_{wall} and ΔPE_{wall}, resp.), the sum of the variation in potential energy and the kinetic energy of the projectile ($\Delta PE_{proj} + KE_{proj}$). KE_{proj} comprises of the rotational and translational kinetic energies. The initial value of the former component is nil for these two impacts but will be varied in the following. This Figure also shows the cumulative energy dissipated by friction at all interfaces (D_f) and by plasticization in the concrete blocks (D_p). The sum of all these energy terms is also plotted (Σ). All these quantities are normalised by the projectile kinetic energy at impact, $KE_{proj}(t_0)$.

It is assumed that, at the projectile-wall contact, energy dissipation only occurs in the impacted concrete block, which is consistent with the absence of projectile damage observed after the experiments. In these plots, kinetic energy accounts for both translational and rotational energies. For presentation clarity purpose, the contact of the projectile with the soil after it bounced away from the wall is not simulated.

The first observation from Figure 3 is that the sum of all these quantities remained constant, with a nearly nil variation over time. This shows that the energy balance equation (Eq. 13) is respected and demonstrates the soundness of the computation scheme.

The two impact cases exhibit similar trends. The projectile total energy, ΔPE_{proj} + KE_{proj}, sharply decreased at the very impact beginning, as a consequence of its translational velocity reduction associated with the impact with the wall. Just after the projectile lost contact with the wall, its velocity was small, with values of 10.7% the incident velocity for the 520kJ impact, and 5.6% for the 1020kJ one. The variation in concrete blocks potential energy, ΔP_{wall}, remained small with a maximum value reached at 0.15 second approximately (amounting less than 4% the impact energy), suggesting a limited upward displacement of the concrete blocks. By contrast, the concrete blocks kinetic energy, KE_{wall}, experienced a high variation over the first tenths of milliseconds, with a maximum amounting more than 20% the impact energy in both cases. It took more than 0.5 second before the wall kinetic energy was close to zero, with a slightly higher duration for the 1020kJ-impact.

Dissipation by plasticization, D_p, mainly occurred at the very beginning of the impact. Nearly 90% of the total dissipation by plasticization was reached less than 0.1 second after the projectile touched the wall. Dissipation by plasticization lasted longer for the 1020kJ impact case (more than 0.4 second). In contrast, the cumulative energy dissipation by friction, D_f, increased more progressively and stopped increasing after 0.55 second approximately.

For both impact cases, the dominating dissipative mechanism over the whole impact duration reveals to be plasticization. In the end, energy dissipation by plasticization amounted approximately 65% of the incident projectile kinetic energy for both the 520 and the 1020kJ-impact. The remaining was dissipated by friction.

These curves and the derived trends reflect the whole structure response with time and space. Energy dissipation by plasticization traduces the amplitude of the normal impulse between system components. Energy dissipation by friction traduces the amplitude of the relative displacement in the tangential direction between system components, and mainly the concrete blocks and the foundation. Both dissipative mechanisms initiate in the impact vicinity and progressively concern components at further distance, depending on the amplitude of contact force and displacement. Most of the dissipation by plasticization occurs in typically 0.2 second indicating a rapid decrease in contact force amplitude between the blocks throughout the wall. At 0.2 second , the wall still moves and dissipation by friction lasts until sliding on its foundation stops (typically around 0.6 second).

3.3 Discussion

This description clearly shows that quantities associated with energy dissipation in the system describe the whole structure response, with time and space, in a rather condensed and clear manner. The occurrence and respective contribution of the dissipative mechanisms are highlighted.

The predominance of plasticization in energy dissipation after the wall is at rest is evidenced by the ratio between the cumulative energy dissipation by friction, D_f, and the cumulative energy dissipation by plasticization, D_p, referred to as $R_{f/p}$. To some extent, this ratio reflects the relative amplitude of the displacement with respect to the contact intensity (contact force between blocks) over the whole impact duration and whole structure. This ratio takes values of about 0.56 and 0.55 for the 520kJ-

and 1020kJ-impacts respectively. This ratio will be considered in the following as it relates to the whole structure response during the whole impact duration through the relative contribution of the two dissipative mechanisms.

This structure was previously modelled with the finite volume formulation code FLAC3D (Furet et al, 2022). This model accounted for the structure components and geometry in a very realistic way. The constitutive laws accounted for plasticity, in particular for modelling damage to concrete blocks. Energy dissipation was computed with time, considering plasticization and friction as only dissipative mechanisms. Similarly as in this study, the authors concluded that plasticization was the dominating dissipative mechanism, with an average $R_{f/p}$ value of approximately 0.4 considering the two tests. More precisely, this ratio equalled 0.46 and 0.6 for the 520 and 1020kJ impacts respectively. Nevertheless, it is worth highlighting that it was not possible for Furet et al (2022) to access all quantities associated with energy, resulting in a 26% difference between the incident projectile kinetic energy and the sum of all computed terms.

4 Sensitivity of energy dissipation to model parameters

4.1 Models parameters definition

The parameters of the reference model were calibrated using a fine-tuned approach considering the displacement at four points in the structure, at three time instances and during two impact tests at different impact energies. More precisely, the set of best-fit parameters presented in the first row of Table 1 was defined so that the deviation of the model predictions with all these experimental data was minimised. In addition, results presented in Gupta et al (2023) evidenced that decreasing the number and variety of data used for calibrating the model parameters had a significant influence

on the model accuracy in modelling the whole structure response with time. This suggests that the strategy considered for calibrating the model parameters may have a significant influence on energy dissipation quantification by the model.

The dependence of energy dissipation on the model parameters was addressed considering different sets of model parameters that were calibrated from the experimental data following different strategies, with increasing complexity (Table 2). The most simple strategy for calibrating (or validating) a model generally consists in considering the displacement at rest of one point in the structure. The residual displacement at the impact location would have been the relevant data in this purpose but experimental measurements at this location were globally not reliable or not available (Furet et al, 2022). For this reason, we considered the wall displacement after the 520kJ-test at the base, at the Top and at point D (see Fig. 2) which correspond to calibration strategies (CS) 1 to 3 in Table 2. The other strategies consist in considering displacement at different locations in the structure, different time instances (namely "Rest", "Init." and "max" as defined in Gupta et al (2023)) and different impact energies. Overall, strategies 1 to 9 consisted in calibrating the model parameters by comparing the model predictions with different selections of one to three data measured during the real-scale experiments. In other words, each of these nine model was calibrated to provide the best estimate for the displacement at the considered point, time and impact energy. This implicitly means that predictions at other points, times and energy are not expected to be good.

The calibration strategies presented in Table 2 globally give priority to data measured during the 520kJ-test as this kinetic energy is more in accordance with the kinetic energy to which this protection structures is intended. By contrast, the 1020kJ-test corresponds more to an extreme situation in terms of incident projectile kinetic

energy, inducing severe damage to the wall. Also, priority is given to calibrations strategies considering measurements at rest, which is a common practice when calibrating models on a quantitative basis.

For each strategy, the calibration of the model parameters followed the same scheme as for the reference model, making use of the Bayesian interface accelerated with polynomial chaos expansion (PCE) based meta-models (section 2.3). As suggested by Gupta et al (2023), the model parameters value vary significantly depending on the way the model was calibrated (Table 1). In particular, the maximum relative difference in parameter value with the reference model exceeds 50% (e.g., e equals 0.107 for CS8 vs 0.221 for the reference model).

Table 2 Alternative calibration strategies and origin of the calibration data.

Id.	Considered point(s)	Considered time(s)	Considered energy(ies)	Numb. of calib. data
CS1	Base	Rest	520kJ	1
CS2	Top	Rest	520kJ	1
CS3	D	Rest	520kJ	1
CS4	Top	Max.	520kJ	1
CS5	D	Rest	1020kJ	1
CS6	D	Init. + max. + rest	520kJ	3
CS7	D	Rest	520 + 1020kJ	2
CS8	Base + D	Rest	520kJ	2
CS9	Base + D	Rest	1020kJ	2

The nine structure models, corresponding to the nine sets of calibrated parameters, were used to simulate the structure response when exposed to impacts with energies of 520 and 1020kJ. The comparison between the results from the nine models is based on the $R_{f/p}$ ratio, as this ratio reflects the structure response via the relative contribution between the two dissipative mechanisms. More precisely, the relative difference in $R_{f/p}$ for a given model with that computed from simulations with the reference model is presented in Figure 4.

4.2 Comparison of the models predictions

Twelve predictions of $R_{f/p}$ out of eighteen reveal rather good, with a difference with the reference case less than 10% for one impact energy at least. This difference is less than 5% for six predictions. Models that were developed following calibration strategies CS4 and CS8 result in the best predictions among all nine models, with a difference less than 5% for both impact energies. The worse predictions are provided by CS2, CS3 and CS5, with at least one prediction with a difference exceeding 15%.

The four models that were calibrated based on displacement at rest after the 520kJ-test only (CS1, CS2, CS3 and CS8) all underestimate $R_{f/p}$ for the 520kJ impact energy. The fact that all nine models underestimate $R_{f/p}$ for the 1020kJ impact case is not explained. A global trend is observed where a larger number of input data for the calibration results in better predictions. Nevertheless, the fact that differences less than 5% were obtained with the CS4 model, which calibration considered one input data only, suggests this not a strict rule.

Focusing on the calibration strategies resulting in the worst predictions, namely CS2 and CS5, Figure 5 reveals significant difference with the reference model in terms of energy dissipation by friction and by plasticization along the impact. For the 1020kJ-impact case, the models calibrated against CS2 and CS5 underestimate D_f by about 14% and 7% and consequently both models overestimate D_p. For the 520kJ-impact case, D_f is overestimated by one model (CS5) and underestimated by the other (CS2), with a 10% deviation approximately in both cases. The opposite trend is observed focusing on D_p. Last and not least, the differences with the reference model in terms of both D_f and D_p clearly appear from the early stages of the wall response to impact, revealing a significant difference in wall response, and in particular in terms of blocks displacement with time and space.

It can be concluded that models calibrated against a limited number of data generally fail in accurately mimicking the whole structure response with time, which has consequences on the computed energy dissipation.

4.3 Discussion

The results presented in the previous section evidenced that a model calibrated against a limited number of data relating to an impact-induced structure displacement may not be sufficiently precise to provide reliable estimates of energy dissipation terms. For this structure, at least two data appeared minimum in this purpose. This is obviously due to the fact that the model parameters govern the overall dynamic response of the structure, meaning the displacement and load transfer with time and space, with consequences on energy dissipation by both friction and plasticization. Considering the displacement after impact at a single point of this large and complex structure appeared to be inappropriate for calibrating a model used subsequently to estimate energy dissipation. Any model developed in such a purpose, in particular, should thus be calibrated considering a sufficient number of data in relation with the structure response. For example, the displacement at different locations or at different time instances may be considered. This is even more necessary when energy dissipation quantification constitutes the basis of a design method (e.g. Marchelli and Deangeli (2022)).

It is important to remind that, as any model, the numerical model of this structure relies on different simplifications and assumptions which may have consequences on the model predictions in terms energy dissipation. The proposed NSCD model accounts for concrete blocks damage a simple way, with the advantage of a reduced computation time. It has been calibrated so that displacements in time and space can be predicted with good accuracy. Using this model for computing energy dissipation implicitly lies on the hypothesis that all physical processes involved are accounted for. Demonstrating

this hypothesis would require additional measurements, such as the relative speeds of the blocks and their damage, as well as constitutive laws specific to the considered configuration (damage to and friction between highly reinforced concrete blocks under dynamic loading). This is out of reach of this research. It would also be impractical in an operational context, because it would result in excessively long computations. This research is thus based on two working hypothesis which concern the use of a simple model and the dissipative mechanisms.

5 Energy dissipation capacities over a large range of impact conditions

On-site rockfall protection structures are exposed to a wide variety in impact conditions during their normal operation. The induced variability in response of rockfall protection structures is mainly addressed focusing on their deformation or deflection, load transmission and failure (Mentani et al, 2016; Bourrier et al, 2016; Toe et al, 2018; Previtali et al, 2021; Lambert et al, 2021; Douthe et al, 2022; Qi et al, 2022). It is here proposed to address the variability in structure response based on energy dissipation.

5.1 Impact conditions definition

In the previous section, the structure response was addressed considering two impacts in the centre of a 14m long wall, by a projectile with a normal-to-the-wall incident trajectory. These test conditions are consistent with current practices for rockfall protection structures testing, such that prescribed for flexible barriers (EOTA, 2018), but are not representative of field conditions where impacts may occur under very different conditions. These impact tests constitute conformance tests that may not be representative of the on-site structure response. For this reason, and in a similar way as previously done for flexible barriers (Mentani et al, 2016; Toe et al, 2018; Previtali et al, 2023), the investigation of the zig-zag wall response was expanded varying

the impact point location, the translational and rotational velocities of the incident projectile, the deviation of its trajectory with respect to the horizontal axis and with respect to the normal to the wall longitudinal axis. Realistic ranges have been considered for these parameters (Table 3). The range for the impact point location along the vertical axis, z, considered a minimum value equalling the projectile radius at the toe of the wall and a free-board equalling the projectile diam at its top, in accordance with some design practices (Lambert and Bourrier, 2013). The impact point location along the horizontal axis, y was varied from the wall centre to a distance of 3.53 m aside, in accordance with the length of the zig-zag pattern of this wall. The range for the translational velocity, v, corresponds to translational kinetic energies from 130 to 810kJ. The maximum value is about 20% less than the wall nominal capacity (considered to be 1020kJ based on the experiments) to limit severe damage to concrete blocks. The considered ranges for the projectile rotational velocity, Ω, inclination and deviation were derived from the literature (Bourrier et al, 2012; Toe et al, 2018; Noël et al, 2023). The same projectile as in the previous section was considered. The wall length was increased to 28.2 m to limit boundary effects while keeping the computation time reasonable. The structure response description proposed hereafter is thus relevant whatever the impact point location and providing that the wall extremities experience very limited displacement. This condition can be insured on-site with soil abutments or shrouds at the wall extremities.

These impact conditions were also considered by the authors for conducting an inverse analysis of the wall response (Gupta et al, submitted).

Table 3 Model parameters with their considered range and mean value

Param.	Range	Distribution	Unit
Translational velocity (v)	10 - 25	Gaussian	m/s
Rotational velocity (Ω)	0.0 - 5.6	Uniform	rot/s
Impact pos. - along length (y)	0.0 - -3.53	Uniform	m
Impact pos. - along wall height (z)	0.55 - 2.10	Uniform	m
Impact inclination (α)	-60 - +60	Uniform	°
Impact deviation (β)	-45 - +45	Gaussian	°

A Latin hypercube sampling (LHS) method (Lataniotis et al, 2015) was used to generate 300 sets of 6 input parameters from the ranges presented in Table 3 for running simulations with the reference NSCD model of the wall.

5.2 Influence of the impact conditions on the structure response

The variability in structure response varying the impact conditions is illustrated from the 300 simulations results in Figure 6 focusing on the post-impact displacement at the top of the wall. This figure shows the location of the extremity of the structure's vertical connectors, as well as the mean position and the standard deviation of the position in the X- and Y-axis directions of the connectors extremity.

The cloud of points reveals that much larger displacements in the X-axis direction are observed at distance from the wall centre (i.e. when Y ranges from -2 to -4 m. This is also the place where larger variability in displacement with impact conditions is observed. Also, the displacement component along the Y-axis direction is much smaller at the wall centre (Y=0 meter) than that 2.5 m aside. Theses differences in wall displacement according to the impact location along the wall longitudinal axis are attributed to the zig-zag conformation of the wall.

The variability in wall response with the impact conditions is also revealed by the variation in $R_{f/p}$, which value typically ranged from approximately 0.4 to 3.8 over the 300 simulations (Fig. 7). This figure suggests a trend concerning the impact inclination angle where an increase in the impact inclination angle, α, above 0° results in an increase in the minimum value of $R_{f/p}$, meaning an increase in relative contribution of friction over plasticization in total energy dissipation. To a much lesser extent, the minimum value of $R_{f/p}$ seems to vary with y and β.

Apart from α, no clear trend as for the influence of the parameters can be directly derived from this simple figure.

The Sobol indices is much more informative and confirms the influence of α. As for the impact location, $R_{f/p}$ is particularly dependant on the position along the wall longitudinal axis, y, but not on that along the vertical axis, z. In a rather counter intuitive manner, the projectile translational velocity, v, appears to have a very small influence. The influence of the deviation, β, appears significant.

It is worth mentioning that there is a strong dependence between these parameters as confirmed by the fact that the sum of the six Sobol indices significantly exceeds 1.0. This means that the dependence of $R_{f/p}$ on one specific parameter, is influenced by the value of another parameter. For example, the influence of the deviation angle, β, depends on the impact location along the wall longitudinal axis, y, due to the wall zig-zag conformation. The interrelationship also explains why no strong trend can be derived from Figure 8.

The distribution of $R_{f/p}$ was computed from the 300 simulation results complemented with a refined distribution obtained from a specifically developed PCE based meta-model (Fig. 9). This figure shows that the main dissipative mechanism is block plasticization (globally, $R_{f/p} < 1$). Energy dissipation by friction appears to be negligible in some impact cases with $R_{f/p}$ values much less than 0.5. On the contrary, the amount of energy dissipated by friction is more than twice that dissipated by plasticization in other impact situations. Comparison of this distribution with the value of $R_{f/p}$ obtained for the two impact tests against which the model was calibrated (0.56 and 0.55) reveals that these tests conditions favoured even more dissipation by plasticization.

Considering separately cases where the impact energy is higher or lower than 500kJ leads to the same general conclusion (Fig. 9) meaning that the relative contribution of friction with respect to plasticization in energy dissipation is the same whether the projectile velocity is high or low (because its mass was not varied). This comment is in line with the previous one on the influence of the projectile velocity on $R_{f/p}$.

Overall, the prevailing dissipative mechanism appears to be block plasticization, but there exists a strong dependence on the impact conditions. Besides, normal-to-the wall impacts result in $R_{f/p}$ values which do not reflect the average wall dissipative capacities, meaning that the precise assessment of its on-site response in terms of energy dissipation should not be extrapolated from results from such tests.

5.3 Interpretation

The results presented in Figures 7, 8 and 9 convey information of great value for understanding the structure response and assessing its dissipative capacities and, consequently its impact strength.

The displacement of the structure and the amount of energy it dissipates by plasticization and friction depends on the energy that is transferred to the wall during the impact. This amount of energy, referred to as "imparted energy", E_{impart}, is considered equal to the variation in projectile total energy during the impact:

$$E_{impart} = \Delta\big(PE_{proj} + KE_{proj}\big) \tag{17}$$

The ratio between the imparted energy, E_{impart}, and the projectile kinetic energy at impact, $KE_{proj}(t_0)$, ranges from approximately 0.25 to 1 depending on the impact conditions (Fig. 10a). The variability in this ratio is governed by the inclination angle, α, other parameters having negligible influence (Fig. 10b). Lower values of this ratio are observed for high and low values of α (Fig. 10a). This is attributed to the fact that a deviation in trajectory with respect to the normal of the impacted concrete block favours projectile deviation, resulting in a higher projectile rebound velocity and a lower E_{impart}. Such non-normal impacts also result in lower impact forces on the impacted concrete block, and thus to less plastic damage to this block. These two comments are thought to explain the trend as for the influence of α as well as

for the influence of β on the minimum value of $R_{f/p}$ where a lower contribution of plasticization is observed increasing the deviation of the projectile trajectory with respect to the normal to the impacted block.

The virtually negligible influence of the translational velocity on the relative contribution between the two dissipative mechanisms is thought to be due to, first, the Gaussian distribution considered for this value and, second, to the dominating effect of some other parameters.

The $R_{f/p}$ ratio refers to the relative contribution of friction over plasticization in energy dissipation but gives no indication on the amount of energy that is dissipated in the wall. For this reason, evaluating the criticality of an impact in terms of displacement or damage requires also accounting for the amount of energy the wall dissipates during impact, which equals E_{impart}. In other words, a very low, resp. high, value of $R_{f/p}$ will lead to high damage, resp. displacement, only if the energy that is transferred to the wall during impact is high.

The structure efficiency analysis conducted combining $R_{f/p}$ with the imparted energy, E_{impart}, reveals a certain correlation between the two variables, where lower $R_{f/p}$ values are globally associated with impact conditions where E_{impart} is high, and, inversely, higher $R_{f/p}$ values correspond to lower values of E_{impart} (see Fig. 11). Impact situations where the projectile incident trajectory is horizontal, with α values close to 0° , are globally associated with higher E_{impart} values. On the contrary, extreme values of inclination ($\alpha <$ -45° or $\alpha >$ 45° approx.) lead to E_{impart} values less than 400kJ. This figure confirms that downward projectile trajectories (positive α values) tend to favour dissipation by friction, with $R_{f/p}$ values most often higher than 1 while upward projectile trajectories tend to favour dissipation by plasticization, with $R_{f/p}$ values most often lower than 1. These comments are in line with the previous comments on the influence of α on the structure response.

While Figure 9 revealed that the number of impact conditions where dissipation by plasticization was statistically dominating, Figure 11 shows that the structure response over this wide range of impact conditions is such that conditions where plasticization dominates are associated with large amount of energy dissipated by the structure. This leads to the conclusions that the probability for having large damage to concrete blocks is high with this zig-zag conformation wall.

6 Perspectives

In this work, the dissipative capacities of the structure was addressed varying the parameters describing the impact conditions over realistic ranges and considering realistic but rather arbitrary distributions (see Table 1). Important findings derived from figures 9 and 11, in particular, are related to these ranges and distributions. Nevertheless and as previously suggested (Lambert et al, 2021), very different parameter ranges and distributions for the parameters describing the rock blocks trajectories may be observed on real-sites. In addition, there exists some couplings between the parameters. In particular, upward incident trajectories relate to cases where the rock block bounces in the ditch uphill the structure before impacting it. This bounce induces energy dissipation and, for this reason, the rock block translational velocity at impact on the structure is much less on the average than in the case of a block directly impacting the structure with a downward trajectory. These couplings exist and are site-specific but were not accounted for when sampling the 300 sets of input parameters. These comments suggest that the structure dissipative capacity for a given site may statistically differ from that derived from the results presented herein. As a consequence, optimising the structure, for example in terms of conformation, should rather be conducted considering site-specific impact conditions.

For the considered wall, which has a zig-zag conformation, the main dissipative mechanism was associated with concrete blocks damage. The $R_{f/p}$ ratio had an average value of 0.8, meaning that 55% of energy dissipation was due to plastizication. Depending on the impact conditions, the contribution of plasticization on total energy dissipation varied between 20% and 70% approx., corresponding to the highest and lowest observed $R_{f/p}$ values respectively (3.8 and 0.4). Taking advantage of the versatility of this structure type, its design could be improved, in particular considering other conformations. This design optimisation could be based on the $R_{f/p}$ ratio following different strategies in terms of functional requirements. One optimisation strategy could consist in preventing from both large damage to the concrete blocks and large wall displacement whatever the impact conditions. In such an approach, the optimum design would result in a wall for which the ratio $R_{f/p}$ remains within a limited range such that friction and plasticization rather equally contribute to energy dissipation in any case. An other strategy could consist in designing a wall favouring displacement, to prevent damage to concrete blocks, as damage to concrete blocks require work for their replacement. In such a case, the wall geometry could be defined in view of reducing the probability of having a low $R_{f/p}$ value. In this design optimisation process, the value of the ratio should always be complemented with the imparted energy, as large damage or displacement require that the amount of energy transferred to the wall is sufficiently high.

7 Conclusions

Estimating the energy dissipative capacities of structures exposed to impact, among which rockfall protection structures, is of paramount importance for understanding their mechanical response and improving their design. The focus of this work was on a rockfall protection wall made of interconnected concrete blocks for which a numerical model developed under the NSCD framework and calibrated from real-scale impact

experiments was available (Gupta et al, 2023). The method developed to derive the energy dissipated by friction and plasticization from NSCD simulation results was detailed. The response of the structure was addressed in particular in terms of its energy dissipative capacities, considering a wide set of impact conditions.

The main conclusions are:

- the developed computation method ensures energy conservation in the system throughout the simulation, which feature results from the fact that the numerical scheme respects the discrete energy/work balance.
- accurate energy dissipation estimated from simulations requires that the model has been calibrated against several experimental data describing the whole structure impact response with time and space.
- tracking with time the cumulative amount of energy dissipated by friction and that by damage to the concrete blocks provides a description of the whole structure response with time and space.
- the ratio between the contribution of these two dissipative mechanisms, $R_{f/p}$, is proposed to illustrate the whole structure response and assess its energy dissipative capacities.
- damage to concrete blocks is the dominating dissipative mechanism for an articulated-concrete blocks wall with a zig-zag conformation exposed to a wide diversity of realistic impact conditions.

As a perspective, the general approach will be considered for improving the design of such structures when considering site-specific impact conditions, for example for optimising the wall conformation based on the $R_{f/p}$ ratio.

This research focused on a particular type of passive protection structure but the general principle could be applied to any type of structure exposed to impact, and in particular rockfall protective structures in which energy is dissipated by

two mechanisms mainly, as for example flexible barriers or rockfall protection embankments.

References

Acary V, Collins-Craft NA (2023) Energy conservation and dissipation properties for elastodynamics with contact impact and friction, URL https://inria.hal.science/hal-04230941, working paper or preprint

Acary V, Perignon F (2007) Siconos: A Software Platform for Modeling, Simulation, Analysis and Control of Nonsmooth Dynamical Systems. SIMULATION NEWS EUROPE, ArgeSIM/ASIM 17(3/4):19–26. URL https://hal.inria.fr/inria-00522740%0Ahttps://hal.inria.fr/inria-00522740/document

Acary V, Brémond M, Huber O (2018) Advanced Topics in Nonsmooth Dynamics., Acary, V. and Brüls. O. and Leine, R. (eds). Springer Verlag, chap On solving frictional contact problems: formulations and comparisons of numerical methods., p 375–457

Acary V, Bonnefon O, Brémond M, et al (2019) An introduction to Siconos. Technical report

Bourrier F, Berger F, Tardif P, et al (2012) Rockfall rebound: comparison of detailed field experiments and alternative modelling approaches. Earth Surface Processes and Landforms 37(6):656–665. https://doi.org/https://doi.org/10.1002/esp.3202, URL https://onlinelibrary.wiley.com/doi/abs/10.1002/esp.3202, https://onlinelibrary.wiley.com/doi/pdf/10.1002/esp.3202

Bourrier F, Baroth J, Lambert S (2016) Accounting for the variability of rock detachment conditions in designing rockfall protection structures. Natural Hazards https://doi.org/10.1007/s11069-015-2084-0

Castanon-Jano L, Blanco-Fernandez E, Castro-Fresno D (2019) Design of a new energy dissipating device and verification for use in rockfall protection barriers. Engineering Structures 199:109633. https://doi.org/https://doi.org/10.1016/j.engstruct.2019.109633, URL https://www.sciencedirect.com/science/article/pii/S0141029618343116

Dhankal S, Bhandary NP, Yatabe R, et al (2012) Numerical and analytical investigation towards performance enhancement of a newly developed rockfall protective cable-net structure. Natural Hazards and Earth System Sciences 12(4):1135–1149. https://doi.org/10.5194/nhess-12-1135-2012, URL https://nhess.copernicus.org/articles/12/1135/2012/

Di Giacinto D, Grassia L, Capriello G, et al (2020) A novel steel damping system for rockfall protection galleries. Journal of Constructional Steel Research 175:106360. https://doi.org/https://doi.org/10.1016/j.jcsr.2020.106360, URL https://www.sciencedirect.com/science/article/pii/S0143974X20309123

Douthe C, Girardon C, Boulaud R (2022) Sensitivity analysis of the global response of flexible rockfall barriers. Geosciences 12(2). https://doi.org/10.3390/geosciences12020075, URL https://www.mdpi.com/2076-3263/12/2/75

Duan S, Yu H, Xu B (2023) Numerical simulation of a rockfall impacting a gravel cushion with varying initial angular velocity and particle sizes. Granular Matter 33(25). https://doi.org/10.1007/s10035-023-01320-3

Dubois F, Acary V, Jean M (2018) The Contact Dynamics method: A nonsmooth story . Comptes Rendus Mécanique 346(3):247–262. https://doi.org/10.1016/j.crme.2017.12.009, URL https://hal.science/hal-01676287

EOTA (2018) Ead 340059-00-0106: Falling rock protections kits

Frémond M (2017) Collisions in mechanics. Annals of Solid and Structural Mechanics 9:29–56

Frémond M (2002) Non-Smooth Thermo-mechanics. Springer-Verlag, Berlin-Heidelberg

Furet A, Lambert S, Villard P, et al (2020) Response of rockfall protection walls subjected to impact. Revue française de géotechnique https://doi.org/10.1051/geotech/2020017

Furet A, Lambert S, Villard P, et al (2022) Experimental and numerical impact responses of an innovative rockfall protection structure made of articulated concrete blocks . Rock Mechanics and Rock Engineering https://doi.org/doi.org/10.1007/s00603-022-02957-x

Gupta R, Bourrier F, Acary V, et al (2023) Bayesian interface based calibration of a novel rockfall protection structure modelled in the non-smooth contact dynamics framework. Engineering structures 297. https://doi.org/0.1016/j.engstruct.2023.116936

Gupta R, Bourrier F, Acary V, et al (submitted) Inverse analysis of the impact response of a rockfall protection structure: Application towards warning and survey. Engineering Structures URL https://hal.science/hal-04582717

Jean M (1999) The non smooth contact dynamics method. Computer Methods in Applied Mechanics and Engineering 177:235–257. Special issue on computational modeling of contact and friction, J.A.C. Martins and A. Klarbring, editors

Jean M, Moreau JJ (1987) Dynamics in the presence of unilateral contacts and dry friction: a numerical approach. In: Del Pietro G, Maceri F (eds) Unilateral problems in structural analysis. II. CISM 304, Spinger Verlag, p 151–196

Korini O, Bost M, Rajot JP, et al (2021) The influence of geosynthetics design on the behavior of reinforced soil embankments subjected to rockfall impacts. Engineering Geology

Lambert S, Bourrier F (2013) Design of rockfall protection embankments: A review. Engineering Geology 154:77–88. https://doi.org/https://doi.org/10.1016/j.enggeo.2012.12.012, URL https://www.sciencedirect.com/science/article/pii/S0013795213000021

Lambert S, Bourrier F, Gotteland P, et al (2019) An experimental investigation of the response of slender protective structures to rockfall impacts. Canadian geotechnical journal https://doi.org/10.1139/cgj-2019-0147

Lambert S, Toe D, Mentani A, et al (2021) A Meta-Model-Based Procedure for Quantifying the On-Site Efficiency of Rockfall Barriers. Rock Mechanics and Rock Engineering 54(2):487–500. https://doi.org/10.1007/s00603-020-02298-7, URL https://doi.org/10.1007/s00603-020-02298-7

Lataniotis C, Marelli S, Sudret B (2015) Uqlab user manual – the input module. Tech. rep., Chair of Risk, Safety & Uncertainty Quantification, ETH Zurich, report UQLab-V0.9-102

Liang G, Junfa Z, Hanlin L (2022) Impact resistance of unequal diameter double u-shaped metal energy dissipation bearing. Structures 41:404–418. https://doi.org/https://doi.org/10.1016/j.istruc.2022.05.019, URL https://www.sciencedirect.com/science/article/pii/S2352012422003812

Marchelli M, Deangeli C (2022) Towards a codified design procedure for rockfall reinforced earth embankments. Geoingegneria e attività estrattiva pp 50–59. https://doi.org//10.19199/2022.165.1121-9041.0502

Mentani A, Govoni L, Gottardi G, et al (2016) A new approach to evaluate the effectiveness of rockfall barriers. Procedia Engineering 158:398–403. https://doi.org/https://doi.org/10.1016/j.proeng.2016.08.462, URL https://www.sciencedirect.com/science/article/pii/S1877705816326704, vI Italian Conference of Researchers in Geotechnical Engineering, CNRIG2016 - Geotechnical Engineering in Multidisciplinary Research: from Microscale to Regional Scale, 22-23 September 2016, Bologna (Italy)

Ng CW, Zhang D, Choi CE, et al (2023) Analysis of steel baffle installed on footing with dowels for resisting boulder impact. Engineering Geology 312:106956. https://doi.org/https://doi.org/10.1016/j.enggeo.2022.106956, URL https://www.sciencedirect.com/science/article/pii/S0013795222004410

Noël F, Nordang SF, Jaboyedoff M, et al (2023) Comparing flow-r, rockyfor3d and ramms to rockfalls from the mel de la niva mountain: A benchmarking exercise. Geosciences 13(7). https://doi.org/10.3390/geosciences13070200, URL https://www.mdpi.com/2076-3263/13/7/200

Previtali M, Ciantia MO, Spadea S, et al (2021) Multiscale modelling of dynamic impact on highly deformable compound rockfall fence nets. Proceedings of the Institution of Civil Engineers - Geotechnical Engineering 174(5):498–511. https://doi.org/10.1680/jgeen.21.00108

Previtali M, Ciantia MO, Spadea S, et al (2023) Assessing rockfall barrier performance through block propagation codes and meta-models. In: Barla M, Di Donna A, Sterpi D, et al (eds) Challenges and Innovations in Geomechanics. Springer International Publishing, Cham, pp 291–298

Qi X, Zhao L, Hao C, et al (2022) Numerical simulation of dynamic responses of semi-rigid rockfall protection barriers subjected to impact loading at different positions.

Bulletin of Engineering Geology and the Environment 81. https://doi.org/https://doi.org/10.1007/s10064-022-02870-1

Ronco C, Oggeri C, Peila D (2009) Design of reinforced ground embankments used for rockfall protection. Natural Hazards and Earth System Science https://doi.org/10.5194/nhess-9-1189-2009

Toe D, Mentani A, Govoni L, et al (2018) Introducing meta-models for a more efficient hazard mitigation strategy with rockfall protection barriers. Rock Mechanics and Rock Engineering

Volkwein A, Schellenberg K, Labiouse V, et al (2011) Rockfall characterisation and structural protection – a review. Natural Hazards and Earth System Sciences 11(9):2617–2651. https://doi.org/10.5194/nhess-11-2617-2011, URL https://nhess.copernicus.org/articles/11/2617/2011/

Xu H, Gentilini C, Yu Z, et al (2018) An energy allocation based design approach for flexible rockfall protection barriers. Engineering Structures 173:831–852. https://doi.org/https://doi.org/10.1016/j.engstruct.2018.07.018, URL https://www.sciencedirect.com/science/article/pii/S0141029617334053

Yan S, Wang Y, Wang D, et al (2022) Application of eps geofoam in rockfall galleries: Insights from large-scale experiments and fdem simulations. Geotextiles and Geomembranes 50(4):677–693. https://doi.org/https://doi.org/10.1016/j.geotexmem.2022.03.009, URL https://www.sciencedirect.com/science/article/pii/S026611442200036X

Yang G, Qiao F, Lu F, et al (2024) Discrete element modelling of rock-filled gabions under successive boulder impacts. Computers and geotechnics

Yu Z, Zhao L, Liu Y, et al (2019) Studies on flexible rockfall barriers for failure modes, mechanisms and design strategies: a case study of western china. Landslides 16:347–362. https://doi.org/10.1007/s10346-018-1093-y

Zhang L, Lambert S, Nicot F (2017) Discrete dynamic modelling of the mechanical behaviour of a granular soil. International Journal of Impact Engineering 103:76–89. https://doi.org/https://doi.org/10.1016/j.ijimpeng.2017.01.009, URL https://www.sciencedirect.com/science/article/pii/S0734743X16306662

Zhao L, Zhang LJ, Yu ZX, et al (2021) Energy dissipating modes and design recommendation of h-shaped steel baffles subjected to boulder impact. Advanced Steel Construction 17:349–355. https://doi.org/https://10.18057/IJASC.2021.17.4.3

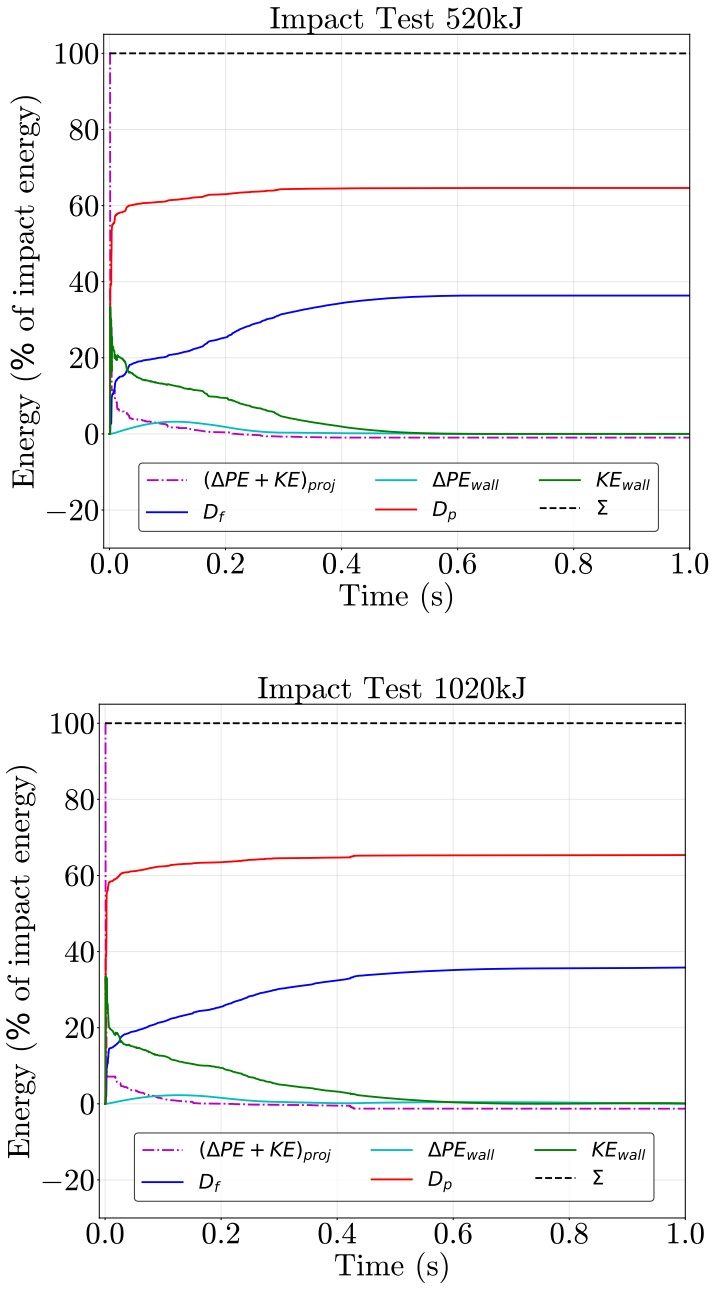

Fig. 3 Energy in the system obtained from the simulation of the structure response to 520- and 1020kJ-energy impacts.

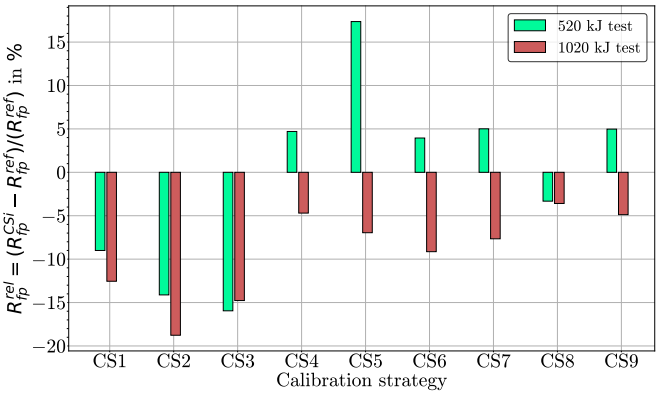

Fig. 4 Relative difference in the ratio of energy dissipated by friction to energy dissipated by plasticization obtained with the models calibrated against the various strategies listed in Table 2 with respect to the ratio value obtained with the reference model.

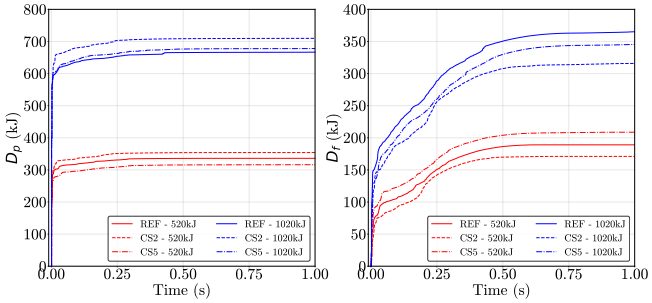

Fig. 5 Energy dissipated in the wall based on simulation results with models calibrated following strategies CS2 and CS5 compared with the reference model: energy dissipated by plasticization, D_p (left) and and energy dissipated by friction, D_f (right).

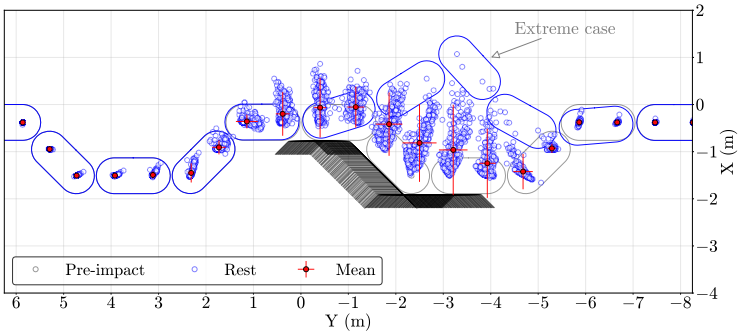

Fig. 6 Displacement at the top of the wall after impacts under different conditions. The dark area shows the range of the impact point location. Axis are defined in Figure 2.

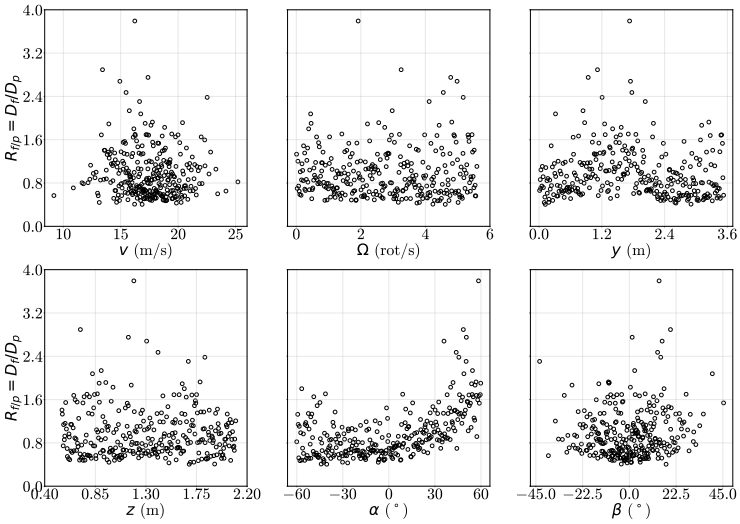

Fig. 7 Dissipation ratio ($R_{f/p}$) vs. each of the six parameters describing the impact conditions for all 300 simulations.

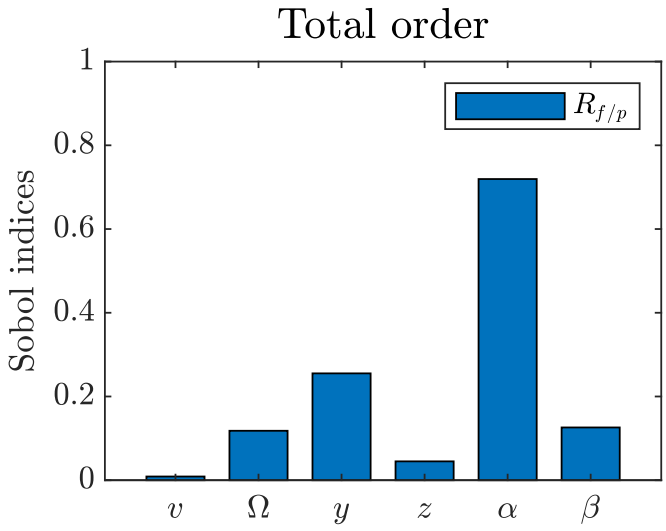

Fig. 8 Total Sobol indices for the dissipation ratio.

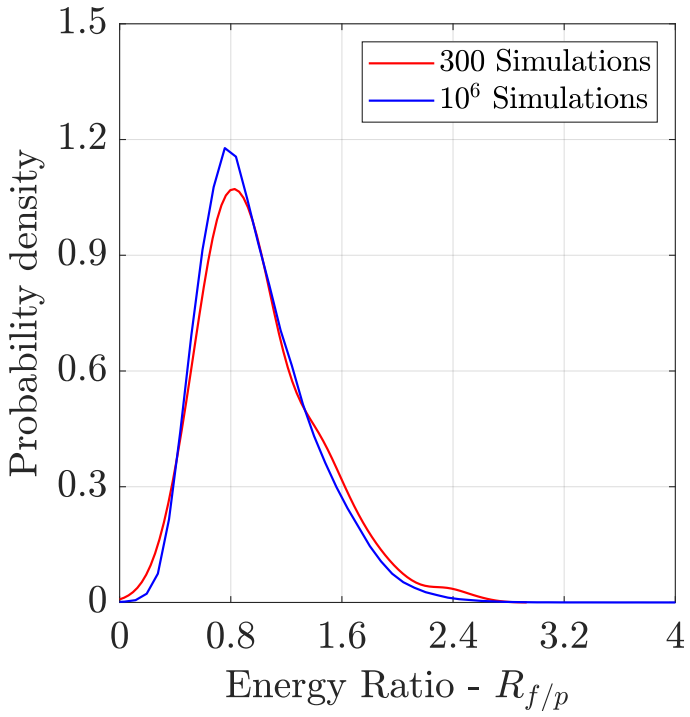

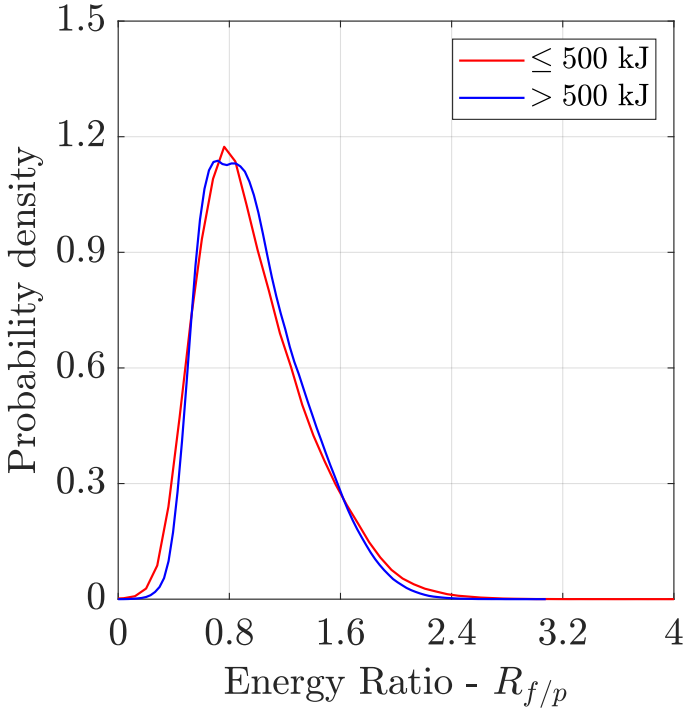

Fig. 9 Distribution of $R_{f/p}$ varying the impact conditions (a) for different number of simulations and (b) for different ranges of incident projectile kinetic energy.

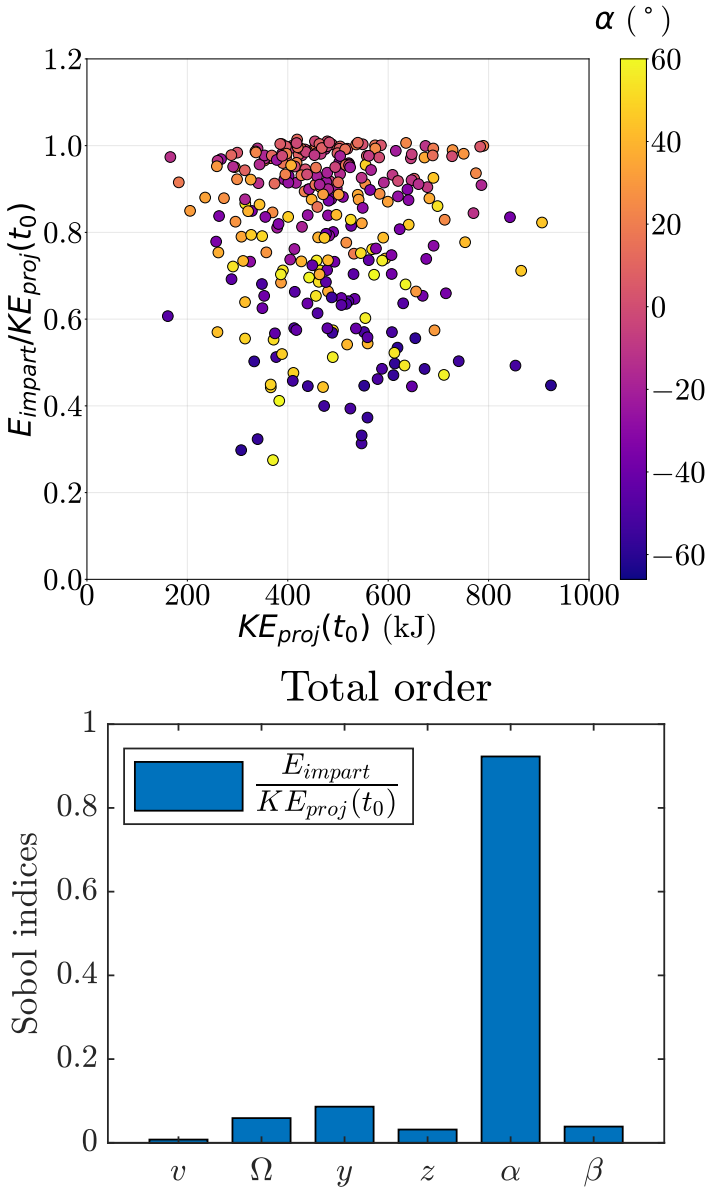

Fig. 10 (a) Ratio of Energy imparted to the wall (E_{impart}) to the projectile kinetic energy at impact, and (b) The total sobol indices of ICPs for this ratio. Computed from the 300 model simulations.

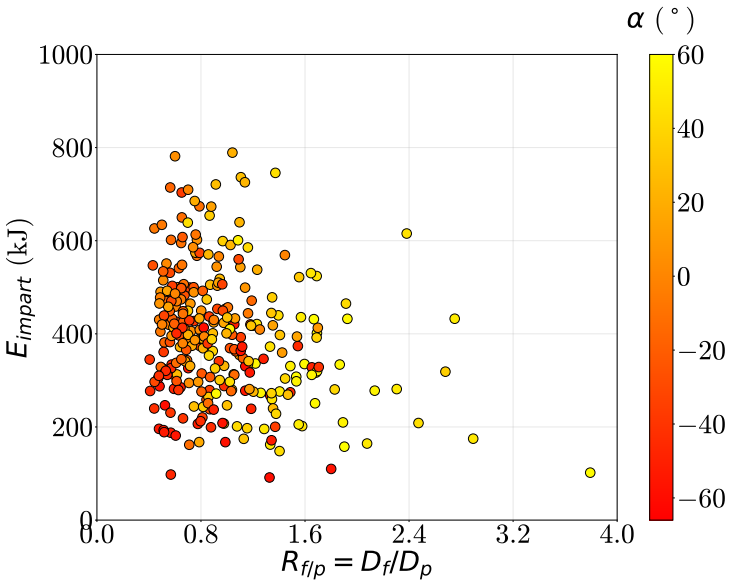

Fig. 11 Energy transferred to the wall and ratio between energy dissipated by friction and energy dissipated by plasticization ($R_{f/p}$). Results from the set of 300 simulations varying the impact conditions.